Structural Sizing of a Tow-Steered Truss-Braced Wing Box Test Article

Brian H. Mason,* Erin K. Anderson,† Alana M. Cardona,‡
Christine V. Jutte,§ and Richard A. Larson**
NASA Langley Research Center, Hampton, VA 23681-2199

Tailoring of composite laminates is traditionally performed by changing the orientation of straight fibers in one or more plies. Modern automated fiber placement machines facilitate placement of bundles of curved fibers (tows) in a process called tow-steering, but additional variables must be used to define the shapes of tow-steered fiber paths. In this paper, the design of a tow-steered truss-braced wing test article called the Structural Wing Experiment Evaluating Truss-bracing 15-ft concept (SWEET-15) is discussed. The SWEET-15 test article is scaled to 18.6% of the span length and chord width of a full-scale vehicle. The test article is designed to withstand +2.5-g (positive limit) and -1.0-g (negative limit) maneuvering loads with a factor of safety of 1.5 under strength and buckling constraints. Design studies were performed using commercial finite element analysis and optimization software in conjunction with a tow-steering modeling tool called ATSCOOL (Automated Tool for Steered COmposite Optimizable Laminates) developed at NASA Langley Research center. A 6.4% weight reduction in the upper cover panels was achieved using a tow-steered layup configuration.

I. Introduction

The NASA Advanced Air Transport Technology (AATT) project is tasked with drastically reducing fuel consumption, noise, and emissions in the next generation of subsonic fixed-wing commercial transport aircraft. AATT is currently considering the ultra-efficient transonic truss-braced wing (TTBW) configuration, as shown in Fig. 1 [1]. One TTBW configuration, the Subsonic Ultra-Green Aircraft Research (SUGAR) configuration includes both a main strut (to help the wing support gravitational and aerodynamic loads) and a jury strut (to prevent buckling of the main strut). This concept is designed to operate efficiently at a cruise speed of Mach 0.80 [2].

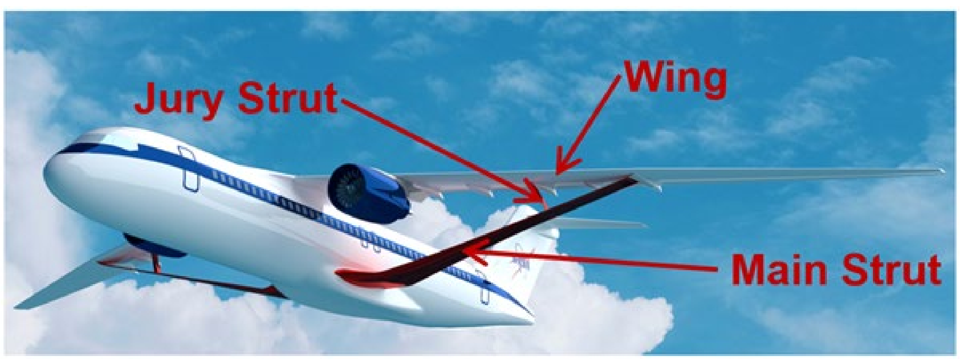

Fig. 1. TTBW concept [1].

---

* Research Aerospace Engineer, Structural Mechanics and Concepts Branch, Mail Stop 190, AIAA Associate Fellow
† Research Aerospace Engineer, Structural Mechanics and Concepts Branch, Mail Stop 190, AIAA Member.
‡ Research Aerospace Engineer, Structural Mechanics and Concepts Branch, Mail Stop 190, AIAA Senior Member.
§ Senior Research Engineer, ViGYAN, Inc., AIAA Member.
** Research Engineer, Analytical Mechanics Associates, AIAA Member

The SUGAR concept has an aspect ratio of 19.6 and offers a 7% to 9% per seat reduction in fuel burn compared to traditional tube-and-wing aircraft with an aspect ratio around 13 [2]. Critical to the success of SUGAR and other TTBW designs are a very thin wing, rapid composite manufacturing processes, and an efficient low-weight structural design. To date, the assessments of TTBW concepts at NASA have been primarily wind tunnel testing with a focus on aerodynamic performance [3, 4] and aeroelastic analysis using low-fidelity structural models [5, 6]. Some more recent structural sizing studies [7, 8] have been conducted at NASA Langley Research Center (LaRC) on a concept called the LaRC TTBW Vision Vehicle. However, structural testing will be needed to ensure that the low-weight structural designs based on current analyses are able to support relevant aerodynamic load cases.

A recent endeavor began under AATT to design, manufacture, and test a 15-ft-long test article representative of a truss-braced wing to support a better understanding of load paths and laboratory testing of a TTBW design. This endeavor is titled SWEET-15 (Structural Wing Experiment Evaluating Truss-bracing 15-ft concept). An additional goal of the SWEET-15 effort is to perform a comprehensive design of a 15-ft truss-braced wing test article, including demonstration of advanced automated fiber placement (AFP) methods, such as tow-steering, composite stitching, and resin infusion capabilities. In AFP, fibers are traditionally placed in straight paths in every ply of the laminate, resulting in laminates that resemble those fabricated via hand layup of material. However, using AFP, fibers can be made to change direction within a ply by programming curvilinear paths into the robotic controls; this approach enables a highly tailored design. Whether straight or curvilinear fiber paths are used, numerous fiber bundles, called "tows," are typically fed from a spool and placed on a tool during AFP. Several tows, all with the same width, placed simultaneously in a preprogrammed path are identified as a "course" of tows. Changing fiber orientation within a ply is called "tow steering." Tow-steered composite designs offer the opportunity for greater stiffness and strength tailoring when compared with standard straight-fiber designs [9-11] of the same mass. SWEET-15 is being manufactured using the Integrated Structural Assembly of Advanced Composites (ISAAC) [12] robotic system at LaRC, as shown in Fig. 2.

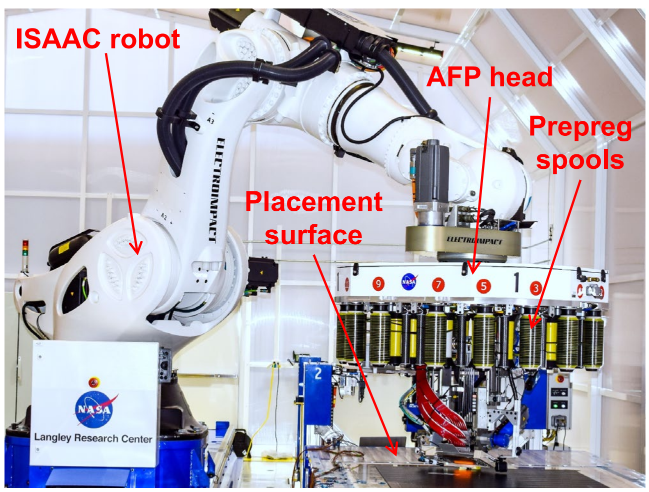

Fig. 2. ISAAC manufacturing robotic system.

The SWEET-15 test article will be assembled at LaRC and will be instrumented with a fiber optic strain sensing system (FOSS) and strain gages. Static and ground vibration testing (GVT) are planned to be conducted at NASA Armstrong Flight Research Center (AFRC) in 2025. In this paper, the initial design process, including tow-steering, for the SWEET-15 test article is described. First, a reference full-scale TTBW finite element model (FEM) is provided, and relevant structural responses are extracted from the model. Next, a FEM of SWEET-15 is created and loads from the TTBW reference FEM are scaled for use as applied loads on SWEET-15. Subsequently the structural sizing process for both standard and tow-steered composite laminates is described. Last, results of the structural sizing are presented, and predicted responses from the SWEET-15 FEM are compared with the full-scale TTBW reference FEM.

II. FEM of LaRC TTBW Vision Vehicle

The structural design of the SWEET-15 test article was a scaled version of the LaRC TTBW Vision Vehicle. Target structural responses were needed to design the test article. Finite element analysis (FEA) was the preferred technique for computational simulation of structural responses. Structural displacements at the wing tip and the wing-to-main-strut interface joint were selected as the target structural response from results generated using the process described in Ref. 7, but in this paper a new FEM was used. These structural responses were obtained from the LaRC TTBW Vision Vehicle FEM shown in Fig. 3. An automated in-house mesh-generation tool called the Conceptual Design Shop (CDS) was used to facilitate creation of a FEM of the wing [13], while the truss structures were created manually using the MSC/PATRAN[††] [14] modeling tool. Structural analyses were performed using the general-purpose FEA code MSC/NASTRAN [15].

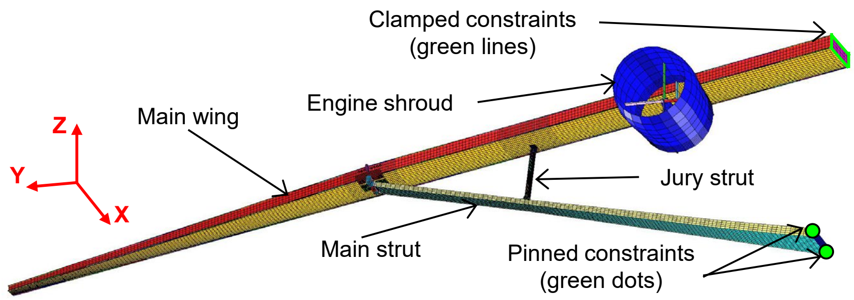

(a) FEM of wing, main strut, jury strut, and engine nacelle

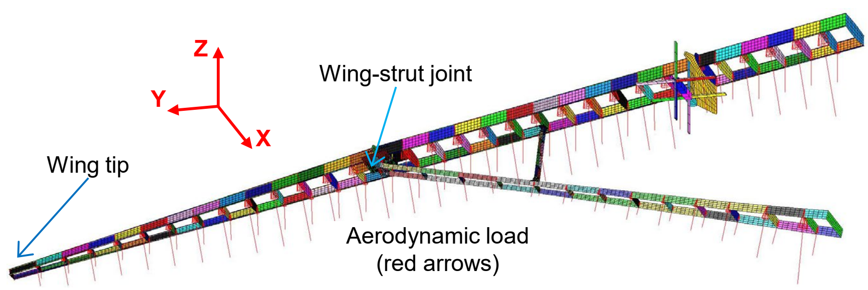

(b) FEM with covers removed for visibility of internal structures

Fig. 3. FEM of LaRC TTBW Vision Vehicle.

Because the SWEET-15 design included only the structural box of the wing and main strut, the leading and trailing edges were excluded from the full-scale FEM. The full-scale LaRC TTBW Vision Vehicle FEM consisted of 21,007 (quadrilateral) shell elements, 1335 beam elements, 47 point masses (accounting for fuel and engine), and 29,972 nodes. In Fig. 3a, the complete FEM and boundary conditions are shown, and in Fig. 3b, the wing and main strut cover panels are removed to show the spars and ribs. The distributed loads summed to half the gross-takeoff weight of the aircraft. Load scenarios included a +2.5-g (positive limit) maneuvering load case and a -1.0-g (negative limit) maneuvering load case, as described in Ref. [8].

The wing and main strut cover panels and spars were modeled as composite laminates of the common carbon-epoxy material system IM7/8552-1 [16], with the assumed material properties given in Table 1. The clevises of the wing-to-strut joints were represented with aluminum shell elements, and beam elements and multi-point constraints were used to represent the bolts. The engine mount and nacelle were given aluminum properties provided in Table 1. The engine and nacelle were included only to provide a load path for the engine weight; hence, these components were defined with zero mass and the component thicknesses were not sized. The engine and nacelle masses were represented by two point-masses located at the engine and nacelle center of gravity (CG) locations and were connected

[††] The use of trademarks or names of manufacturers in this report is for accurate reporting and does not constitute an official endorsement, either expressed or implied, of such products or manufacturers by the National Aeronautics and Space Administration.

to the nacelle with beam elements. Stacking sequences for the wing and main strut laminates were determined by a sizing process described in Ref. 7, and the shell elements with composite properties were designed to satisfy strength (using the Tsai-Hill first-ply failure criterion) and buckling constraints. For this study, the wing and main strut covers were represented with unstiffened solid laminates. For a full-scale TTBW, a stiffened skin configuration may have been more weight efficient, but the timeline constraints of the SWEET-15 endeavor precluded performing such a trade study.

Table 1. Material properties.

Property	IM7/8552 [16]	Aluminum
Weight density, lbf/in.^{3}	0.05714	0.100
Elastic Modulus – Longitudinal, Msi	22.99	10.60
Elastic Modulus – Transverse, Msi	1.30	10.60
Shear Modulus, Msi	0.68	3.98
Poisson's Ratio	0.316	0.330
Tensile Strength – Longitudinal, ksi	362.69	N/A
Tensile Strength – Transverse, ksi	9.29	N/A
01 Strength – Longitudinal, ksi	248.94	N/A
Compressive Strength – Transverse, ksi	41.44	N/A
Shear Strength, ksi	13.22	N/A

A linear static analysis of the LaRC TTBW Vision Vehicle FEM was conducted in MSC/NASTRAN, and the joint and tip displacements in the z-direction are given in Table 2. The ratio of the tip displacement over the joint displacement, 5.47, was used as a target constraint in sizing the composite laminates of the SWEET-15 FEM, as described in Section V. The displacement ratio was based only on the +2.5g (positive limit) maneuvering load as a simplification of the constraint for optimization.

Table 2. Structural response of TTBW under +2.5g (positive limit) maneuvering load case.

Response	Wing-spar joint	Wing tip
Displacement, z-direction, in.	6.81	37.28
Displacement, z-direction, % span length	0.70%	3.84%

III. FEM of Initial SWEET-15 Test Article

As mentioned in the previous section, the SWEET-15 test article was scaled to 18.6% of the span length and chord width of the LaRC TTBW Vision Vehicle. The SWEET-15 wing box depth and main strut box depth were scaled to 25% and 33% of the LaRC TTBW Vision Vehicle, respectively. The increased box depth was a manufacturing requirement to allow for installation of fiber optic sensors and strain gages. The planform dimensions of SWEET-15 are given in Fig. 4. For manufacturing purposes, the geometry of the SWEET-15 was simplified compared to the complex curvature of the LaRC TTBW Vision Vehicle such that the wing and main strut boxes have flat upper and lower cover panels. In addition, for manufacturing purposes, the wing was divided into an inboard and an outboard section. The inboard section of the wing box had a constant but swept cross-section, while the outboard section tapered in chord width and depth while maintain the sweep angle. The SWEET-15 main strut was a single linearly tapered box section, whereas the main strut in the LaRC TTBW Vision Vehicle had multiple tapered sections.

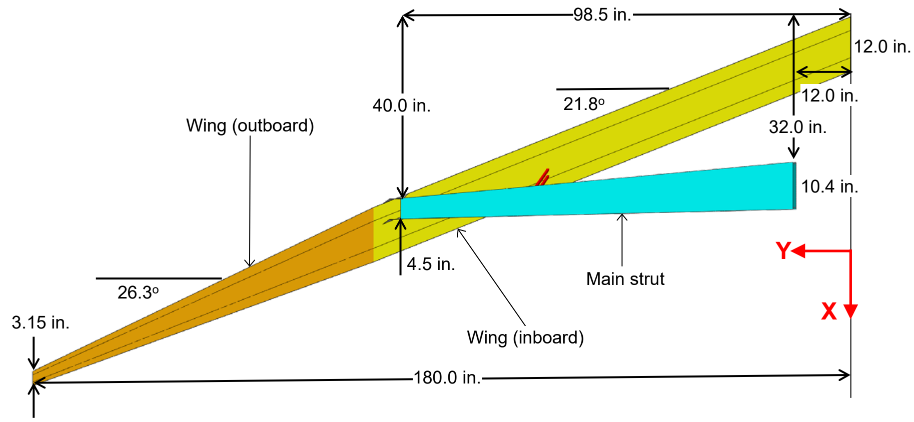

Fig. 4. Planform dimensions of SWEET-15.

The initial FEM of SWEET-15 test article is shown in Fig. 5. The FEM had 43,818 quadrilateral shell elements, 18 beam elements (representing the jury strut), and 43,596 nodes. The wing was composed of upper and lower cover panels and a forward and aft tubular spar (with rectangular cross-sections, as illustrated in Fig. 5b). The upper and lower cover panels were each divided into four sections, as shown by color in Fig. 5a. The main strut was a stitched composite box structure connected to the wing with a metallic joint and comprised three zones of varying skin thickness as shown in Fig. 5a with distinct colors. The joint, shown in Fig. 5c, consisted of metallic spar extensions on the main strut that were attached to two metallic clevises with multipoint constraints (representing a bolt). Surface-to-surface kinematic coupling constraints were used to connect the wing cover panels to the tubular spars and to connect the joint clevises to the lower cover panel of the wing. For the FEM of this test article, general-purpose FEA code ABAQUS [17] was selected for analysis because the code includes fracture mechanics modeling features (including the virtual crack closure technique and cohesive zone elements). However, fracture mechanics studies were beyond the scope of this paper.

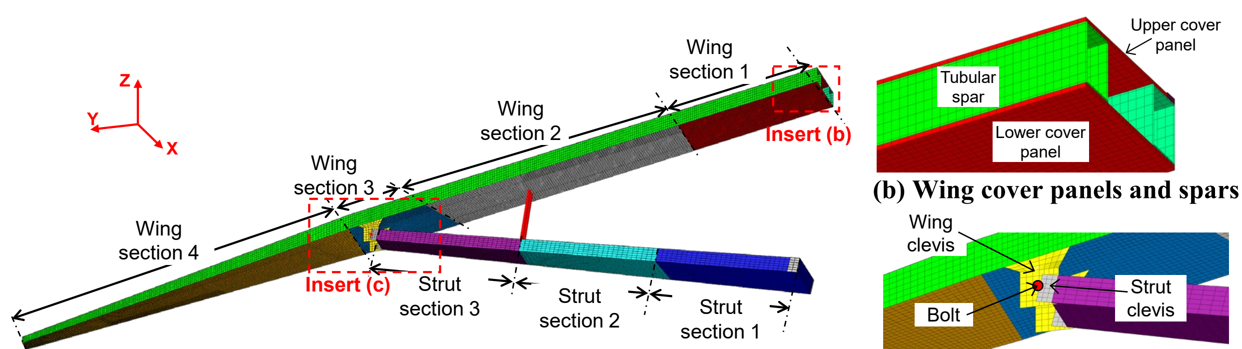

(a) FEM of wing, main strut, and jury strut. **(b) Wing cover panels and spars** **(c) Wing-strut joint**

Fig. 5. FEM of SWEET-15.

IV. Scaling of Loads from LaRC TTBW Vision Vehicle to SWEET-15

In the LaRC TTBW Vision Vehicle FEM, loads were applied at the forward and aft edges of the 32 wing ribs and 9 main strut ribs. For the SWEET-15 test article, the LaRC TTBW Vision Vehicle loads were redistributed to six forward and six aft locations on the wing and two forward and two aft locations on the main strut to reduce the number of load introduction points in the planned test. Scaling of the applied loads from the LaRC TTBW Vision Vehicle to the size of SWEET-15 was necessary for the two models to have similar stress and stability (buckling) responses. As an initial evaluation of load scaling, the wing was considered as a cantilevered rectangular beam of length L with cross-sectional width b and box height h (with moment of inertia I). Each beam dimension was scaled by a scale factor α, and the applied tip load F was scaled by a load factor β. The initial and scaled bending stress (σ) for the cantilever wing are given by Equations 1 and 2, respectively. Equation 2 was solved for the load factor to yield Equation 3.

$$\sigma_{initial} = \frac{FL}{I}\left(\frac{h}{2}\right) = \frac{FLh}{2\left(\frac{bh^3}{12}\right)} = \frac{6FL}{bh^2} \tag{1}$$

$$\sigma_{scaled} = \frac{6\beta F(\alpha L)}{\alpha b(\alpha h)^2} = \frac{\alpha\beta}{\alpha^3}\frac{6FL}{bh^2} = \frac{\beta}{\alpha^2}\sigma_{initial} \tag{2}$$

$$\beta = \frac{\sigma_{scaled}}{\sigma_{initial}}\alpha^2 \tag{3}$$

For the initial and scaled stresses to be the same, Equation 4 has to be satisfied

$$\beta = \alpha^2 \tag{4}$$

The initial and scaled buckling load factors λ (for a beam with a Young's modulus of E) are given by Equations 5 and 6, respectively.

$$\lambda_{initial} = \frac{F}{\frac{\pi^2 EI}{4L^2}} = \frac{4FL^2}{\pi^2 E\frac{bh^3}{12}} = \frac{48F}{\pi^2 E}\frac{L^2}{bh^3} \tag{5}$$

$$\lambda_{scaled} = \frac{48\beta F}{\pi^2 E}\frac{(\alpha L)^2}{\alpha b(\alpha h)^3} = \frac{\alpha^2\beta}{\alpha^4}\frac{48F}{\pi^2 E}\frac{L^2}{bh^3} = \frac{\beta}{\alpha^2}\lambda_{initial} \tag{6}$$

Similarly, when the buckling load factors were set equal, the load factor was the same as in Equation 4. Using the 18.6% length scale factor, an initial approximated load factor of 3.44% was obtained with Equation 4.

A simplified study was conducted by running a few analyses using load factors near 3.44% and comparing the joint and tip displacements of the SWEET-15 FEM to the percent values in Table 2. An FEA with a load factor of 4.1% was used to produce a joint and tip displacement of 0.7% and 4.0%, respectively, which was considered to be an adequate representation with the results from the TTBW reference FEM. With the 4.1% load factor, the applied loads on the SWEET-15 at the six wing stations and two main strut stations are given in Fig. 6a and 6b for the +2.5-g (positive limit) maneuvering and -1.0-g (negative limit) maneuvering load cases, respectively. The applied load values in Fig. 6 represent point forces on the forward and aft edges of the wing and main strut in the z-direction from the root edge of the wing (y=0 in.) to the wing tip (y=180 in.), which would correspond to actuator-applied loads in the test. Also, the first point at the wing forward station (at about y=30 in.), the load is reduced to represent the inertial effect of the engine mass.

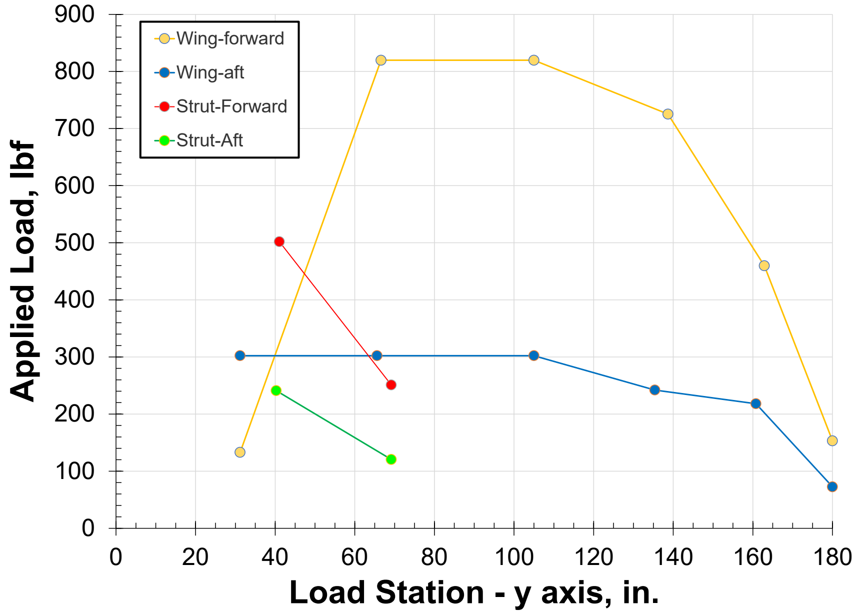

(a) +2.5-g (positive limit) maneuvering load

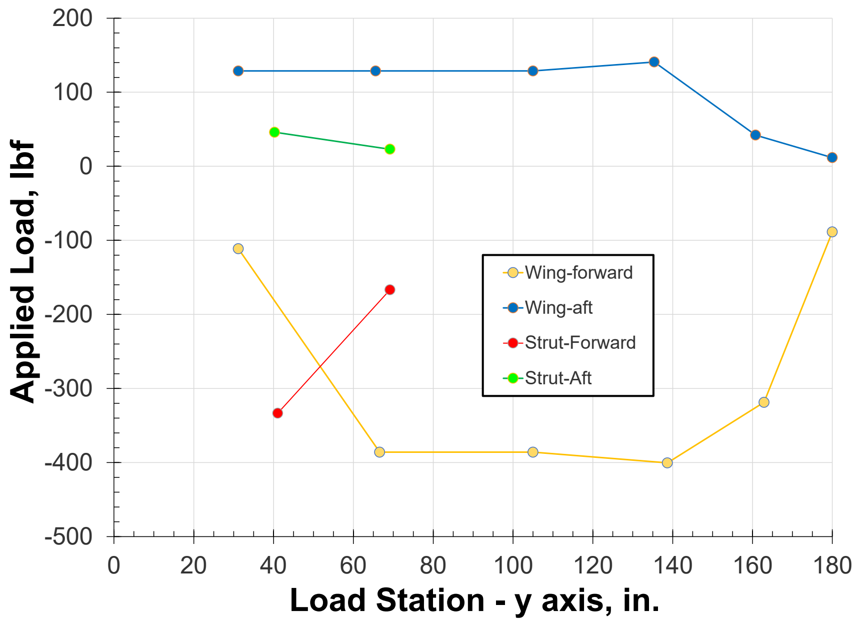

(b) -1.0-g (negative limit) maneuvering load

Fig. 6. Applied loads for SWEET-15.

V. Structural Sizing Approach

A two-phase optimization approach was used to determine the stacking sequences for the wing cover panels and tubular spars. In the first phase, the laminates were designed using standard straight fibers, as shown in Fig. 7a. In the second phase, the upper cover panel was sized in two sections (inboard and outboard) using tow-steered laminates, as illustrated in Fig. 7b. The stitched quasi-isotropic laminates in the main strut were not sized to minimize weight, but were set to constant values of 8, 7, and 6 stacks (each stack is 0.0424 in. thick) in the root, middle, and tip sections of the main strut, respectively, based on initial sizing results.

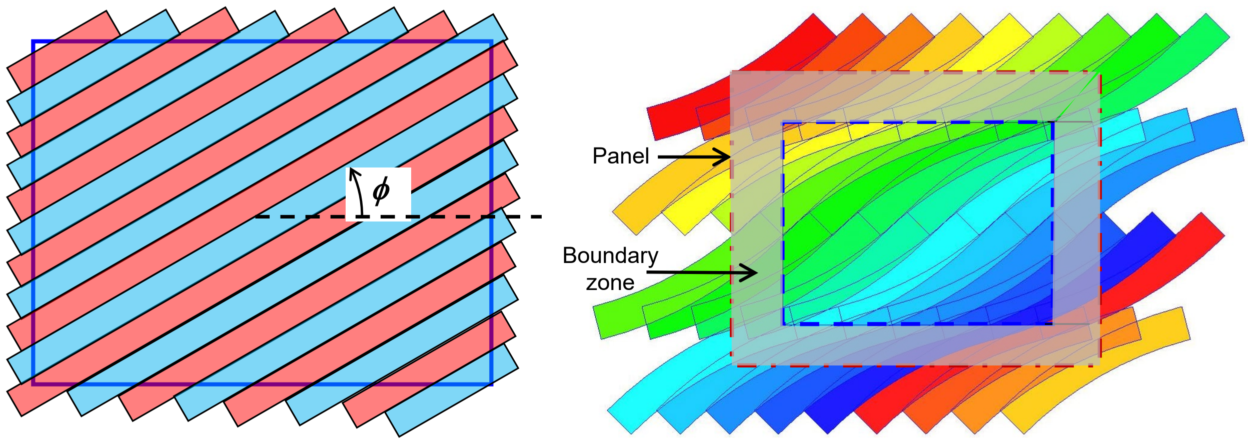

(a) Standard straight-fiber laminate **(b) Tow-steered laminate**

Fig. 7. Comparison of standard and tow-steered laminates.

The LS-OPT software framework [18] was selected as a design optimization tool to size metallic shell thicknesses and to define composite laminate stacking sequences in the ABAQUS FEM. The LS-OPT software can be set up to run any command-line-driven analysis code, such as a Python script or a FEA code. The software can also be used to perform optimization on a response surface representing the selected objective as a function of the design variables, or it can perform optimization using direct simulation with a genetic algorithm. Due to differences between the response surfaces and the actual simulated values observed in early stages of this study, direct simulation with a genetic algorithm was selected.

LS-OPT was used to determine the minimum structural weight of the wing, subject to buckling and strength (Tsai-Hill criteria) constraints under the +2.5-g (positive limit) maneuvering and -1.0-g (negative limit) maneuvering load cases discussed in Section II, with an applied factor of safety of 1.5. The ratio of the tip displacement to the joint displacement of 5.47, derived from displacements in Table 2, was used to set up an additional constraint to ensure the SWEET-15 FEM and the TTBW reference FEM had similar deformed shapes. This ratio was constrained within a range of 5.27 to 5.67 (5.47 ±0.20) and constituted a stiffness constraint.

For the initial straight-fiber sizing study (first phase), the design variables were the ply thicknesses for the symmetric composite laminate representing the wing covers and spars. For each composite laminate, integer variables (denoted with 'n') were used to define the number of plies for each orientation angle used in the laminate. For example, the number of plies for 0º, 45º, and 90º orientations were denoted as n0, n45, and n90, respectively. Quasi-isotropic ([±45/0/90]) stacks of plies were used symmetrically as outer plies in each laminate. The number of stacks was the minimum value of plies n0, n45, or n90 associated with the laminate. The remaining plies (the differences between the minimum and the remaining two out of three: n0, n45, and n90) were placed as innermost plies in the laminate. As shown in Figs. 5a and 5b, the upper and lower cover panels were each divided into four sections with identical stacking sequence, and a constant stacking sequence was used for each of the spars (forward and aft), resulting in 10 laminate sections. The three integer variables, n0, n45, and n90, were assigned per composite laminate section, bringing the total number of design variables to 30. A Python script was used to map the array of design variables to ABAQUS shell section property cards.

In the second phase, the upper cover panel of the SWEET-15 was designed with tows placed along a curved path, in a process called tow-steering. Tow-steered laminates have been shown to have improved buckling resistance over traditional laminates [9-11], so only the buckling-critical upper cover panel of the SWEET-15 test article was selected for tow-steering design. A recently developed tool called ATSCOOL (Automated Tool for Steered COmposite

Optimizable Laminates) [19] was used to define a tow-steered composite laminate both in the ABAQUS FEM and in a CAD file that is imported into the manufacturing control scripts for the ISAAC robotic system. To limit the number of variables in the design process, the steered tows were defined using a mirrored circular arc pattern (MCAP) as shown in Fig. 8. With MCAP, a primary curve was defined using five variables: the radius of curvature (R), the orientation angle of the directional, mirroring axis (ϕ), the half-wavelength (d) of the repeated arc, and the x- and y-locations (x0 and y0) of the origin of the primary curve, as shown in Fig. 8a. To create the tow placement paths of a single tow-steered course, the arc shown in Fig 8a was repeated as many times as necessary to cover the desired panel area, with the center of curvature mirrored about the directional axis (d) as the arc propagated across the panel. A blue tow propagated from a pink base arc chain is shown in Fig. 8b. Three variables were used to define the pattern for repeating the initial curved tow: a shift angle (ψ), a shift distance (s), and a course width (w), as shown in Fig. 8b. The shift distance in Fig. 8b represented a minimum value (s_{min}) that was allowed by the ATSCOOL tool, for which neighboring tows are allowed to touch at one (repeated) location and overlap everywhere else. The value of s_{min} was a function of the shape of the primary curve, shift direction, and course width, and was computed internally by ATSCOOL. Within the ATSCOOL input file, a gap variable (g) was defined as the difference in the shift distance and the minimum shift distance ($g = s - s_{min}$).

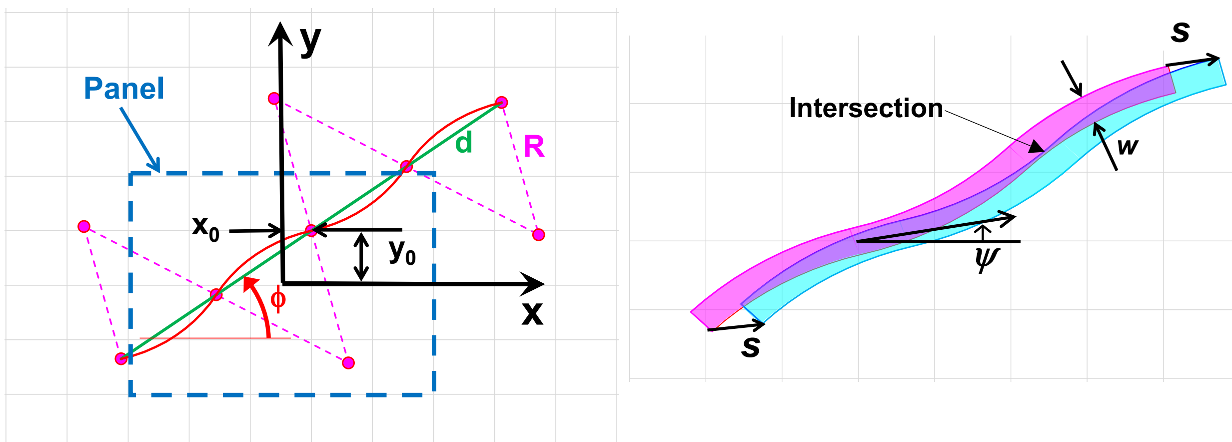

(a) Variables defining primary curve **(b) Variables defining tow placement**

Fig. 8. Geometry of steered tows.

Manufacturing constraints were applied to the tow-steering design process. A minimum radius of curvature of 30 in. was used in order to prevent defects related to curling of the tows at the edge of a course during AFP [20]. The stacking sequences of all tow-steered laminates were symmetric. The initial two plies of the laminates were a +45º and a -45º ply; because during AFP, straight tows place on a pristine tooling surface much more uniformly and with fewer defects than steered tows. Steered tows were placed in $\pm\phi$ pairs with identical radii of curvature, shift directions, and gaps, but different offsets. The use of offsets enabled staggering of the courses. As part of best practices, for the ISAAC system, at least a single straight fiber ply was required between each tow-steered fiber pair, and the laminate required at least one pair of 0º and 90º plies to reduce the likelihood and magnitude of panel warpage during the consolidation process.

VI. Results of Structural Sizing

Multiple optimization cycles were performed using the LSOPT software. Initial cycles were conducted with the 10 laminate zones constrained to be quasi-isotropic layups to envelope a range of ply thicknesses for each zone and to quickly determine a design that satisfied the buckling, strength, and stiffness constraints. Approximately 20 iterations of the generic algorithm with a population size of 30 per iteration were used to reach an optimum. Each FEA (preprocessing, analysis, and post-processing) required about 4 minutes, so the optimization process required about 40 hours. A second LSOPT run was conducted in the initial phase using a tighter range of ply thicknesses, but for this case, orthotropic designs were allowed and utilized all 30 design variables. The sized straight-fiber designs are shown in Fig. 9a for the upper cover panel and Fig. 9b for the lower cover panel. The forward and aft spars of the wing were sized to have 18 and 16 plies, respectively.

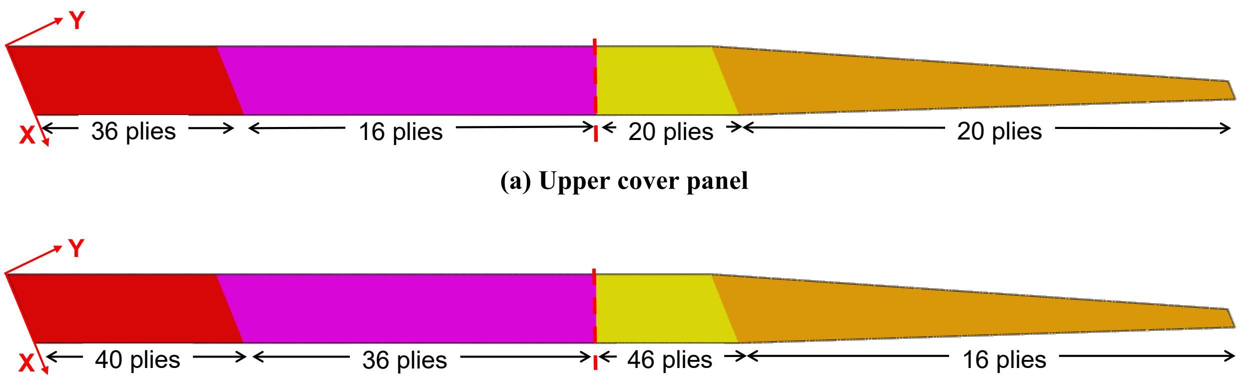

(a) Upper cover panel

(b) Lower cover panel

Fig. 9. Thickness of standard (straight-fiber) laminates from initial sizing.

In the second phase of the structural sizing process, laminates in the upper cover of the wing were replaced with tow-steered designs. The upper cover was sized as two panels using wing sections 1 and 2 for the inboard panel and wing sections 3 and 4 for the outboard panel (see Fig. 5). The stacking sequences from the first phase were used to estimate the number of plies needed for the tow-steered designs (20 to 24 plies). Due to the constraint on the minimum number of straight-fiber plies discussed in the previous section, only two pairs of tow-steered plies were used in the symmetric stacking sequence for each panel. Design was performed using the following stacking sequence: $[\pm 45/\pm A/\pm T_1/\pm B_1/\pm T_2/\pm B_2/\pm C]_S$, where A, B_1, B_2, and C are straight fiber plies and T_1 and T_2 are tow-steered plies. Values for the angles are given in Table 3, where the subscript "Half" represents a single ply at the center of the laminate and "null" represents a switch indicating that this angle ply can be deleted. The sized laminates are shown in Fig. 10. In Figures 10a and 10b, the centerlines of the course paths for the tow-steered plies are plotted on top of a thickness map of the laminate on the inboard and outboard panels, respectively. The nomenclature of superscripts in the stacking sequences in the tow-steered layers include the same radius of curvature (R) and half-wavelength (d) defined above and now include a gap distance (g). A FEM of the inboard and outboard panels is shown in Figures 10c and 10d, respectively, with the thickness of the shell panels illustrated three-dimensionally. The thickness of the shell panels is scaled by a factor of 10 for visibility on these plots, but the associated fringe reflects actual thickness measurements.

Table 3. Range of variables used in tow-steered designs.

Variable	Angle Plies, degrees	Cross Plies, degrees	Other Plies, degrees
A	±15, ±30, ±45, ±60, ±75	0/90, 90/0	0, 0_2, 90, 90_2, null
B	±15, ±30, ±45, ±60, ±75	0/90, 90/0	0, 0_2, 90, 90_2
C	±15, ±30, ±45, ±60, ±75	0/90, 90/0	0_{Half}, 0, 0_2, 90_{Half}, 90, 90_2
T	±5, ±10, ±15, ±20, ±25, ±30, ±35, ±40, ±45, ±50, ±55, ±60, ±65, ±70, ±75, ±80	N/A	0_2

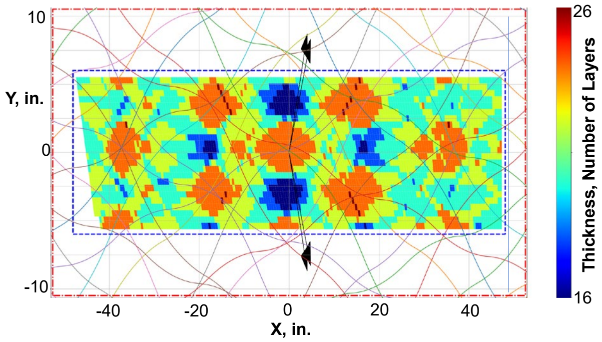

24 plies $[\pm45/\pm15/\pm25^{R36d18g4.0}/0_2/\pm10^{R40d12g3.5}/0/90]_s$
(a) Thickness of inboard panel and centerlines of curved tows (from ATSCOOL tool)

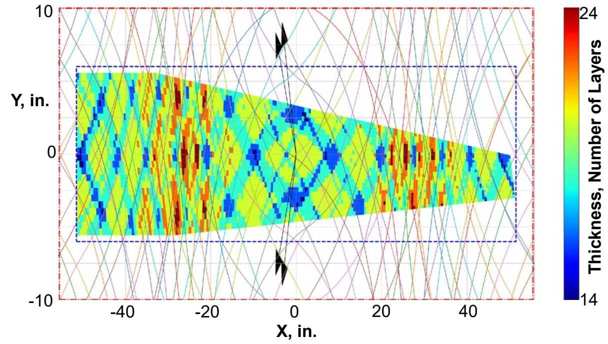

20 plies $[\pm45/90/0/\pm35^{R37d30g1.5}/90/\pm50^{R35d29g3.5}/90]_s$
(b) Thickness of outboard panel and centerlines of curved tows (from ATSCOOL tool)

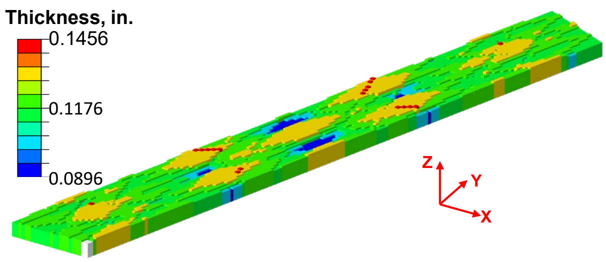

(c) Thicknesses of inboard panel scaled by a factor of 10

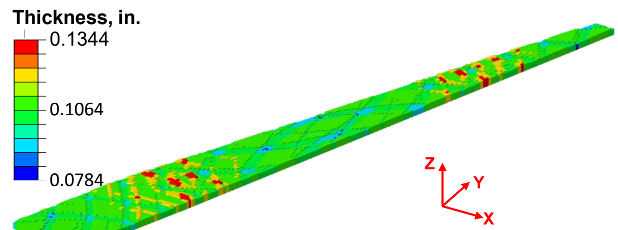

(d) Thicknesses of outboard panel scaled by a factor of 10

Fig. 10. Thickness of tow-steered upper cover laminates.

Results from phase 1 (straight fibers) and phase 2 (tow-steering) of the sizing process are presented in Table 4 and Fig. 11. Application of the -1.0-g (negative limit) maneuvering load induced a compressive loading in the lower cover panel, but the lowest eigenvalue for this load case was 1.804, which was above the 1.0 limit; so, buckling was not critical for the lower cover panel. Therefore, the lower cover panels (which are not resized in phase 2) were sized for strength (requiring a Tsai-Hill failure index below 1.0). As shown in Fig. 12, the highest Tsai-Hill failure index occurred in the lower cover panel vicinity of the wing-main strut joint. Tsai-Hill values for the upper cover panel were much lower than the lower cover, hence the upper cover panel is not shown in Fig. 12. The inboard section of the upper cover panel was sized for stiffness matching of the SWEET-15 FEM with the TTBW reference FEM, and neither strength nor buckling were critical constraints for this section, but the tow-steered design was 7.9% lighter than the standard design. The outboard section of the upper cover panel was buckling critical, as the lowest eigenmode occurred in this section, as illustrated in Fig. 13. The deformations shown in Fig. 13 were scaled to 10% of the wingspan for visibility. The tow-steered design of the outboard section of the upper cover was 3.9% lighter with a 13.9% higher buckling load compared to the standard design. The total weight improvement for both upper cover panels was 6.4%

Table 4. Structural response of sized panels with and without tow-steering.

Location	Panel Weight, lbf	Maximum Tsai-Hill Failure	Minimum Buckling Eigenvalue
Lower cover inboard, straight-fiber	12.09	0.996	Greater than 7.0
Lower cover outboard, straight-fiber	6.18	0.751	1.804
Upper cover inboard, straight-fiber	8.04	0.457	1.337
Upper cover inboard, tow-steered	7.42	0.561	1.226
Upper cover outboard, straight-fiber	4.48	0.420	1.001
Upper cover outboard, tow-steered	4.30	0.504	1.140

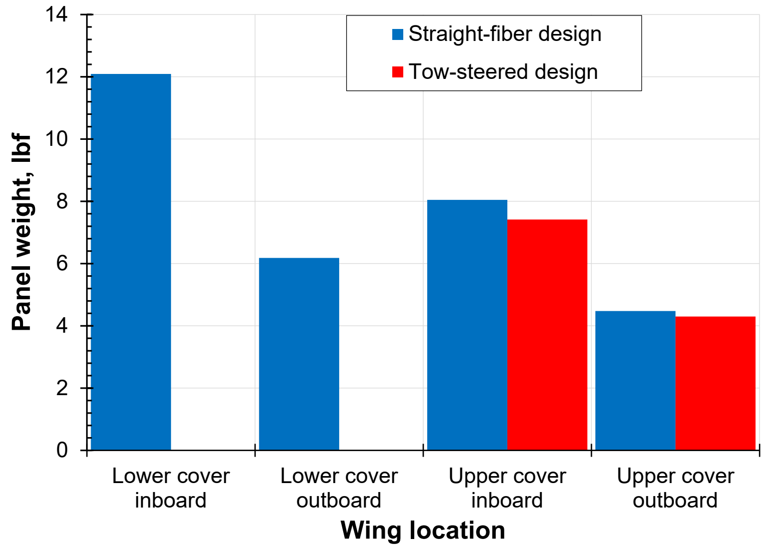

Fig. 11. Panel weight comparisons.

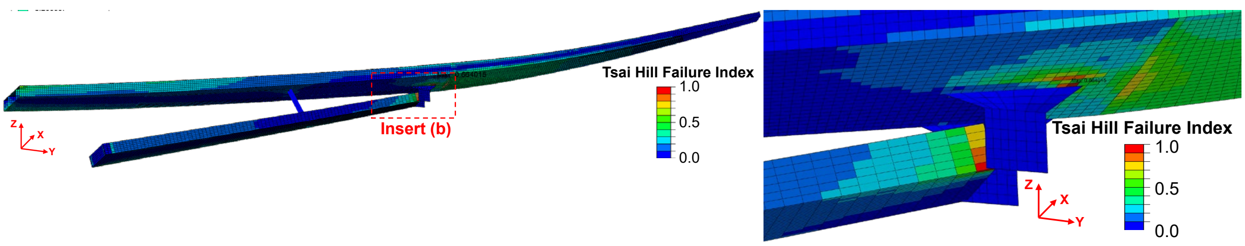

(a) Failure index for SWEET-15 **(b) Failure index at wing-main strut joint**

Fig. 12. Tsai-Hill failure index for SWEET-15 FEM.

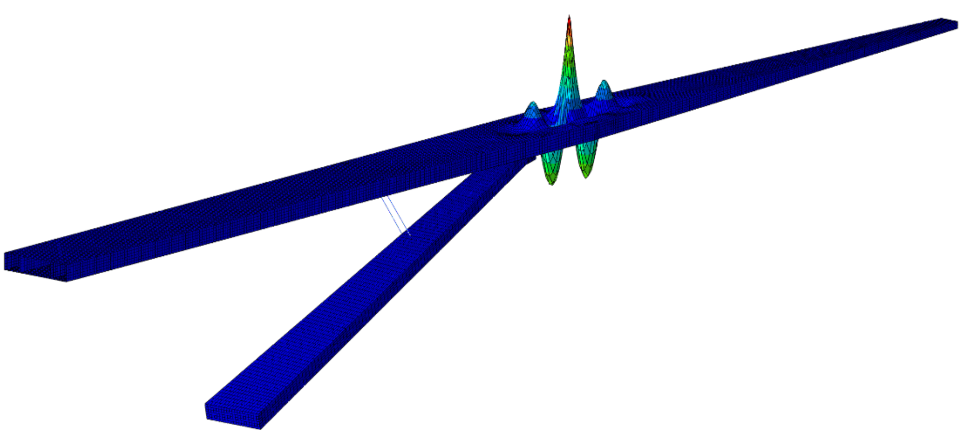

Fig. 13. Mode shape of SWEET-15 FEM at lowest eigenvalue for 2.5-g (positive limit) maneuvering load.

VII. Refined FEM of SWEET-15 Test Article

The initial FEM of SWEET-15 test article was refined as additional details pertaining to the test fixtures and joints were developed. Among these details were improved modeling of the wing-strut joint and the root fixtures for the strut and main wing, as shown in Fig. 14. This FEM has 204,910 quadrilateral shell elements, 12 beam elements (representing bolts at the joints), 10,800 hexahedral solid elements (representing the root fixtures), and 219,844 nodes.

The wing was divided into three sections, as shown by color in Fig. 14a. As an additional detail, ply drops were included in the lower cover to transition between sections with different laminate thicknesses. Additionally, an integral stiffener ran the length of the inboard and outboard sections in the lower cover, as shown in Fig. 14b. The integral stiffener consisted of a 1-in.-wide band of 0º tows placed intermittently within the laminate during AFP. In the integral stiffener, approximately one band of tows was placed per two plies in the laminate. The joint, shown in Fig. 5c, consisted of metallic spar extensions on the main strut that were attached to two metallic clevises with multipoint constraints to two bolts represented by beam elements. Structural analyses for the refined FEM were performed using the general-purpose FEA code MSC/NASTRAN to have software compatibility with AFRC.

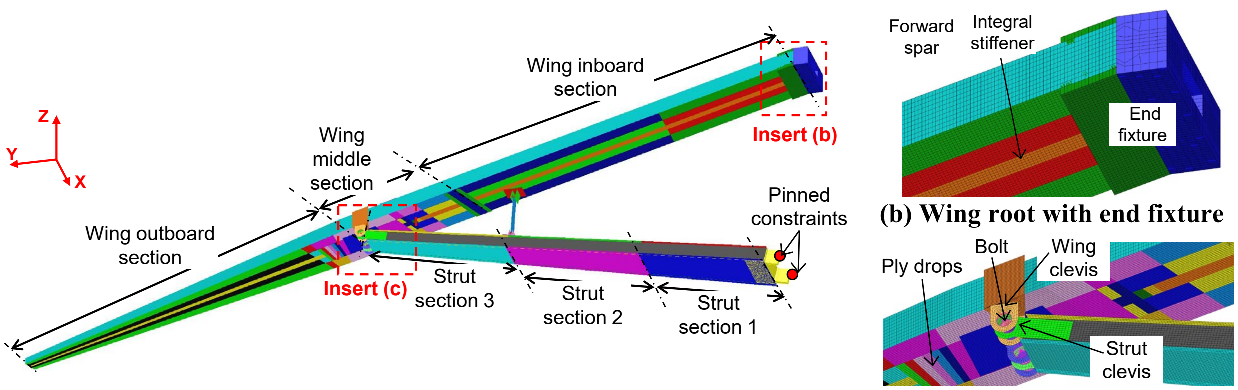

(a) FEM of wing, main strut, and jury strut. **(b) Wing root with end fixture** **(c) Wing-strut joint**

Fig. 14. Refined FEM of SWEET-15 test article.

VIII. Results of Structural Sizing of Refined Model

Structural sizing of the refined model was accomplished using a two-step process. First, an initial linear static and buckling analysis of the refined model was performed using the sizing results from Section VI. Thicknesses of the metallic joint components were increased as needed to satisfy von Mises stress limits. The inclusion of the integral stiffener in the lower cover permitted a slight reduction of the laminate thicknesses in the lower cover from the values in Fig. 9b to the values shown in Fig. 15.

The structural sizing approach described in Section VI was used to size the thicknesses of the upper cover panels. Both upper cover panels were tow-steered using variables defined in Section VI (stacking sequence **$[\pm 45/\pm A/\pm T_1/\pm B_1/\pm T_2/\pm B_2/\pm C]_S$** using variables defined in Table 3). The resulting tow-steered laminates are shown in Fig. 15a. The weight, failure index, and buckling values for the upper covers in the refined model under ultimate load are given in Table 5. The inboard and outboard panels from the refined model were 5.0% and 12.9% heavier than the panels from the initial model, for a total weight increase of 7.5%. The weight increase in the inboard panel was attributed to increased stresses around the bolt holes in the end root fixture (as shown in Fig. 16b) which were not modeled in the initial model. For the outboard panel, a heavier design was chosen as a balance between increasing the buckling load and more closely matching the thickness of the inboard panel to reduce discontinuity between the inboard and outboard panel thickness at the interface. However, the lowest buckling load for the redesigned upper cover panels was 27.9% higher than the buckling load for the design based on the initial model. Due to project schedule constraints, a standard, straight-fiber laminate representation of the upper cover panels was not sized, so comparison of the tow-steered to standard design was not performed for the refined model.

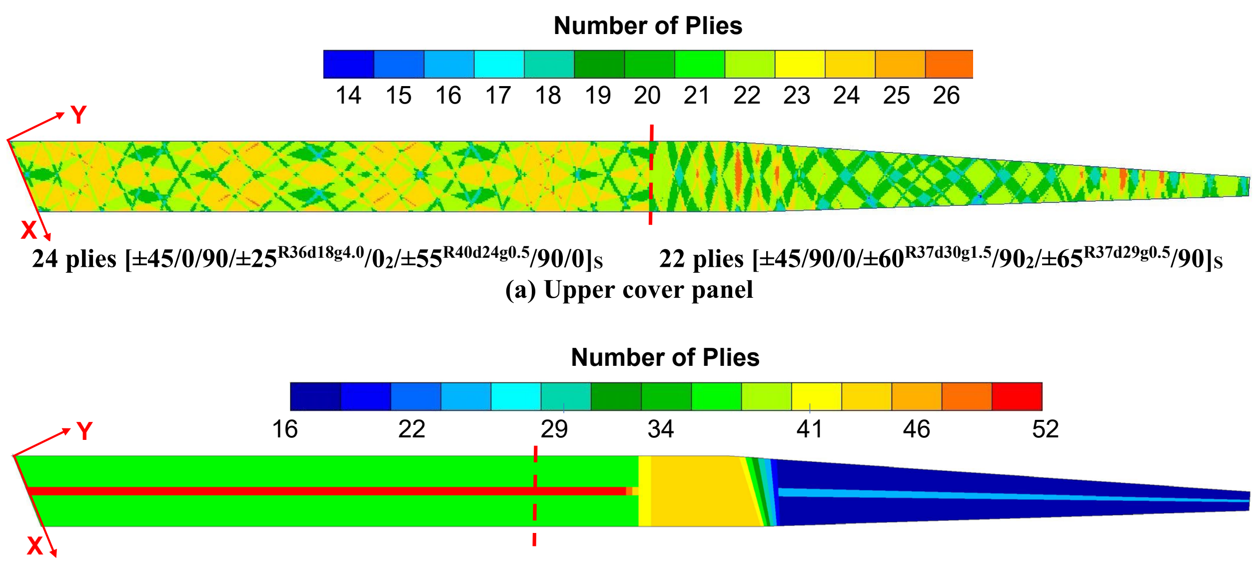

(a) Upper cover panel

(b) Lower cover panel

Fig. 15. Thickness of standard laminates from initial sizing.

Table 5. Structural response of sized panels with and without tow-steering.

Location	Panel Weight, lbf	Maximum Tsai-Hill Failure	Minimum Buckling Eigenvalue
Initial, upper cover inboard, tow-steered	7.42	0.561	1.226
Refined, upper cover inboard, tow-steered	7.79	0.941	1.458
Initial, upper cover outboard, tow-steered	4.30	0.504	1.140
Refined, upper cover outboard, tow-steered	4.81	0.471	1.571

In Fig. 16, the highest Tsai-Hill failure index values in the lower cover and upper cover are shown. For the upper cover, the highest Tsai-Hill failure index value of 0.941 occurred near a bolt hole at the aft edge of the root end fixture. In the lower cover, the highest Tsai-Hill failure index of 0.946 occurred near a bolt hole at the aft edge of the base of the wing clevis of the aft wing-strut joint, as shown in Fig. 16b. Mode shapes for the lowest three eigenmodes are presented in Fig. 17. The deformations in Fig. 17 were magnified by 10% of the wingspan for visibility. The first two modes occurred in the upper cover between the root and the load fixture representing the engine mount. The third mode occurred in the upper cover just outboard of the wing-strut joint. All eigenvalues were above the 1.0 limit.

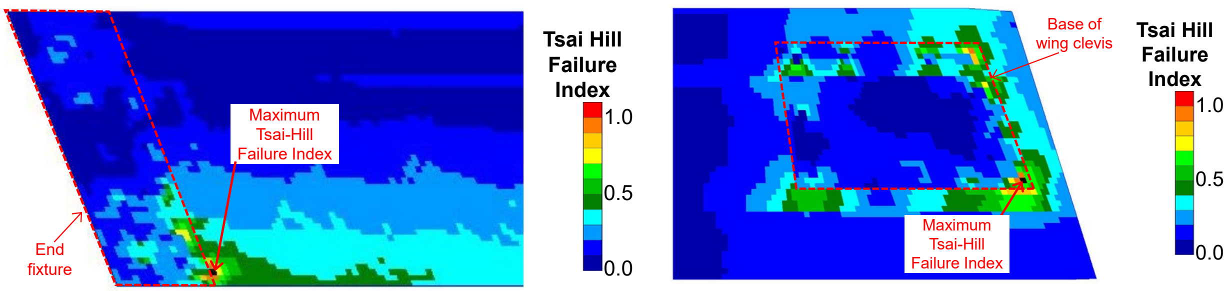

(a) Failure index at root of wing (upper cover) **(b) Failure index at wing-main strut joint (lower cover)**

Fig. 16. Tsai-Hill failure index for SWEET-15 FEM.

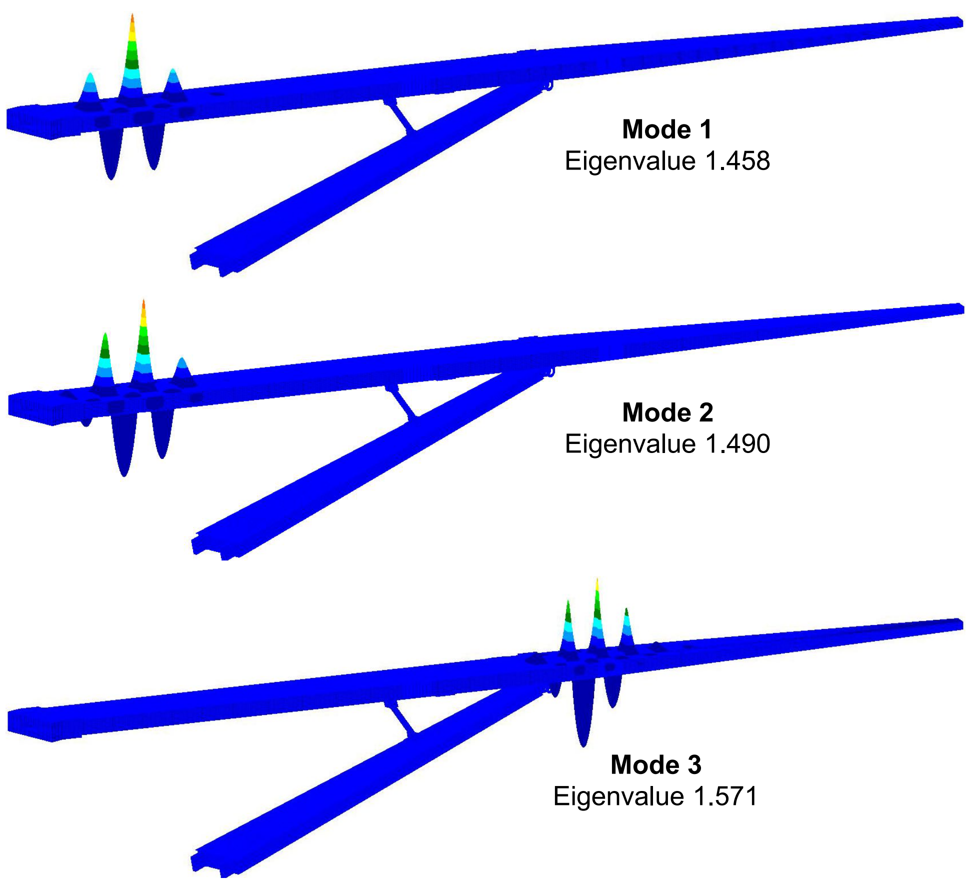

Fig. 17. Lowest three mode shapes of refined SWEET-15 FEM for 2.5-g (positive limit) maneuvering load.

In Fig. 18, the as-built upper cover panels are shown. Both panels were built at the ISAAC facility using AFP. Curves representing the steered tows were generated by the ATSCOOL tool and these curves were used to program the course paths performed at ISAAC along with the straight fiber paths. Overlaps and gaps between the steered tows are visible in both panels in Fig. 18, where the overlaps create peaks along the surface, and gaps create the surface valleys.

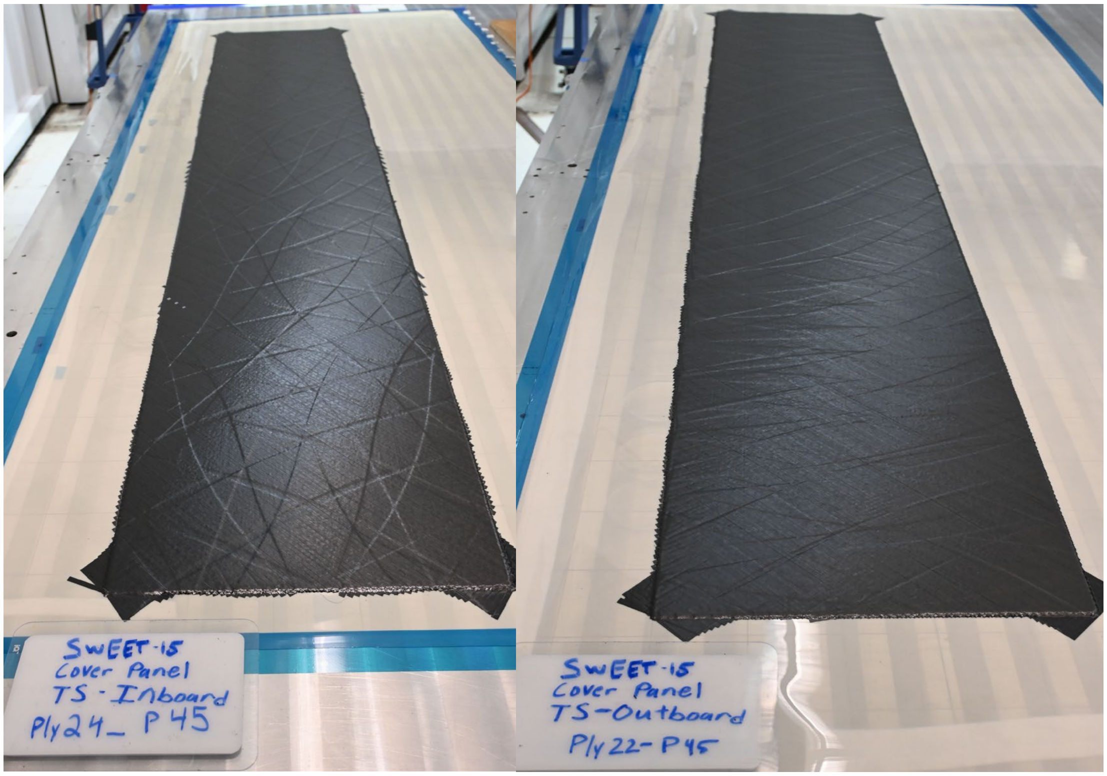

(a) Inboard panel before cure **(b) Outboard panel before cure**

Fig. 18. As-built tow-steered upper cover panels.

IX. Concluding Remarks

In this paper, the optimization process to create the wing portion of a subscale 15-foot long TTBW test article assembly, the SWEET-15, was presented. Two phases of design were evaluated, where the first phase was based on a traditional straight-fiber layup configuration primarily using the composite wing and metallic components, and the second phase was on the design of the tow-steered layup used in the upper covers of the wing. From this study, a 6.4% weight reduction in the upper cover panels was achieved using a tow-steered layup configuration in the SWEET-15 wing when compared to the initial straight-fiber model.

Refinements to the FEM of SWEET-15 test article were performed, and the upper cover panels were redesigned based on the improved modeling of the joint and fixtures. With the addition of modeled fixtures and joints, the new design was 7.5% heavier than the initial tow-steered design, but the buckling load for the new design was 27.9% higher than the initial design. Due to project constraints, an optimized straight-fiber design of the refined model was not generated.

Finally, the two upper cover tow-steered panels were successfully manufactured at ISAAC using the geometry curves generated by the ATSCOOL tool. The other components of the SWEET-15 test article are currently being manufactured with the intention of testing at AFRC in 2025.

X. Acknowledgements

The authors would like to acknowledge the guidance of Ms. Dawn Jegley and Dr. Adam Przekop in developing the concepts and plans for this projected. Additionally, we would like to acknowledge Dr. Danny Drake and W. Allen Waters for their early work on the nonlinear behavior of the truss-braced wing model.

XI. References

[1] Gipson, L., "NASA Plans for Subsonic Flight Demonstrator," *https://www.nasa.gov/aeroresearch/nasa-plans-for-subsonic-flight-demonstrator,* NASA, April 24, 2023.

[2] Harrison, N. A., Hoffman, K., Lazzara, D. S., Reichenbach, E. Y., Sclafani, A. J., and Droney, C. K., "Subsonic Ultra Green Aircraft Research: Phase IV Final Report – Volume 1 Mach 0.80 Transonic Truss-Braced Wing High-Speed Design Report," NASA/CR–20220016017, Vol. 1, October 2023.

[3] Harrison, N. A., Gatlin, G. M., Viken, S. A., Bevar, M., Dickey, E. D., Hoffman, K., and Reichenbach, E. Y., "Development of an Efficient M=0.80 Transonic Truss-Braced Wing Aircraft," AIAA Paper 2020-0011, AIAA SciTech 2020 Forum, Orlando, FL, January 6-10, 2020.

[4] Maldonado, D., Viken, S. A., Housman, J. A., Hunter, C. A., Duensing, J. C., Frink, N. T., Jensen, J. C., McMillin, S. N., and Kiris, C. C., "Computational Simulations of a Mach 0.745 Transonic Truss-Braced Wing Design," AIAA Paper 2020-1649, AIAA SciTech 2020 Forum, Orlando, FL, January 6-10, 2020.

[5] Fugate, J., Nguyen, N. T., and Xiong, J., "Aero-Structural Modeling of the Truss-Braced Wing Aircraft Using Potential Method with Correction Methods for Transonic Viscous Flow and Wing-Strut Interference Aerodynamics," AIAA Paper 2019-3028, AIAA Aviation 2019 Forum, Dallas, TX, June 17-21, 2019.

[6] Gur, O., Bhatia, M., Schetz, J. A., Mason, W. H., Kapania, R. K., and Mavris, D. N., "Design Optimization of a Truss-Braced Wing Transonic Transport Aircraft," *Journal of Aircraft*, Vol. 47, No. 6, 2010.

[7] Anderson, E. K., Cardona, A. M., and Mason, B. H., "Structural Sizing of a Composite Transonic Truss-Braced Wing," AIAA Paper 2023-2083, AIAA SciTech 2023 Forum, National Harbor, MD, January 23-27, 2023.

[8] Jutte, C. V., Mason, B. H., and, Bartels, R. E., "Simplified Applied Loads of a Transonic Truss-Braced Wing Derived from Computational Fluid Dynamics," AIAA Paper 2024-2811, AIAA SciTech 2024 Forum, Orlando, FL, January 8-12, 2024.

[9] Hyer, M. W. and Lee, H. H., "The Use of Curvilinear Fiber Format to Improve Buckling Resistance of Composite Plates with Central Holes," *Composite Structures*, Vol. 18, 1991, pp. 239-261.

[10] Nagendra, S., Kodiyalam, A., Davis, J. E., and Parthasarathy, V. N., "Optimization of Tow Fiber Paths for Composite Design," Proceedings of the 36th AIAA/ASME/ASCE/AHS/ASC Structures, Structural Dynamics, and Materials (SDM) Conference, AIAA-1995-1275, New Orleans, LA, April 1995.

[11] Tatting, Brian F., and Gürdal, Zafer, "Design and Manufacturing of Elastically Tailored Tow Placed Plates," NASA/CR 2002-211919, August 2002.

[12] NASA ISAAC Fact Sheet, FS-2016-12-273-LaRC, 2021.

[13] Mason, B. H. and Quinlan, J. R., "Conceptual Design Shop: A Tool for Rapid Airframe Structural Modeling," AIAA Paper 2018-2001, AIAA SciTech 2018 Forum, Kissimmee, FL, January 8-12, 2018.

[14] *PATRAN Software Package*, Ver. 2016, MSC Software, Santa Ana, CA, 2016.

[15] Anonymous, NASTRAN Analysis Quick Reference Manual, MSC Software, Santa Ana, CA.

[16] Zahn, A., and Lovejoy, A. E., "Test and Analysis Correlation of Standard and Hybrid Standard/Thin-ply Composite Notched Test Specimens," AIAA Paper 2020-0478, AIAA SciTech 2020 Forum, Orlando, FL, January 6-10, 2020.

[17] *Abaqus Software Package*, Ver. 6.14, Dassault Systèmes Simulia Corp., Pawtucket, RI, 2012.

[18] Stander, N., Eggleston, T., Craig, K., and Roux, W., "LS-OPT User's Manual A Design Optimization and Probabilistic Analysis Tool for the Engineering Analyst," Version 2, October 2003.

[19] Mason, B. H., Cardona, A. M., Anderson, E. K., and Jegley, D. C., "A Tool for Defining Tow-Steered Laminates for Finite Element Grids," NASA/TM-20230015301, November 2023.

[20] Cardona, A. M., Jegley, D. C., and Lovejoy, A. E., "Manufacturing Trials of Integrally Stiffened Composite Panels Using Automated Fiber Placement," Society for the Advancement of Materials and Process Engineering (SAMPE) Conference and Exhibition, Seattle, WA, April117, 2023.